Non-modal growth of perturbations in density-driven convection in porous media

SAIKIRAN RAPAKA[1], SHIYI CHEN[1,2],
RAJESH J. PAWAR[3], PHILIP H. STAUFFER[3]
AND DONGXIAO ZHANG[4]

[1]Department of Mechanical Engineering, Johns Hopkins University, Baltimore,
MD 21218, USA
saikiran@jhu.edu

[2]COE & CCSE, Peking University, Beijing, China

[3]EES-6, Los Alamos National Laboratory, Los Alamos, NM 87544, USA

[4]Department of Civil and Environmental Engineering, University of Southern California,
Los Angeles, CA 90089, USA

In the context of geologic sequestration of carbon dioxide in saline aquifers, much interest has been focused on the process of density-driven convection resulting from dissolution of CO_2 in brine in the underlying medium. Recent investigations have studied the time and length scales characteristic of the onset of convection based on the framework of linear stability theory. It is well known that the non-autonomous nature of the resulting matrix does not allow a normal mode analysis and previous researchers have either used a quasi-static approximation or solved the initial-value problem with arbitrary initial conditions. In this manuscript, we describe and use the recently developed non-modal stability theory to compute maximum amplifications possible, optimized over all possible initial perturbations. Non-modal stability theory also provides us with the structure of the most-amplified (or optimal) perturbations. We also present the details of three-dimensional spectral calculations of the governing equations. The results of the amplifications predicted by non-modal theory compare well to those obtained from the spectral calculations.

1. Introduction

Carbon dioxide storage in deep saline aquifers is considered to be one of the most promising ways of mitigating greenhouse gas emissions (see IPCC 2005). Saline formations are usually characterized by a high porosity and permeability, are filled with non-potable water and are usually covered by a layer of very low-permeability caprock on the top. This technology has already been implemented in a few operations around the world. The most notable of these is at the Sleipner West field in Norway, operated by Statoil Corporation. About 2800 tons per day of CO_2 extracted from the field is being stored underground at a depth of 1000 m, and is being monitored by seismic surveys.

Under the conditions at which it is injected, CO_2 is in a supercritical state and its density is lower than that of the water in the medium. The injected carbon dioxide migrates upwards due to buoyancy and settles as a layer under the low-permeability caprock at the top of the aquifer. The carbon dioxide can migrate laterally along the caprock, which leads to the possibility of leakage due to either fractures or other wells.
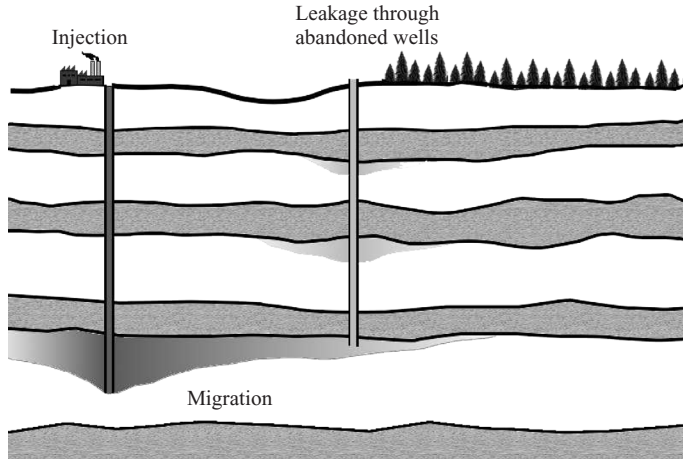
FIGURE 1. Schematic of carbon dioxide injection, migration and leakage during geologic storage.

A schematic of the injection, migration and leakage processes is shown in figure 1. Carbon dioxide also begins to slowly dissolve in the water. The water with dissolved carbon dioxide has a density slightly greater (by about 1 %) than that of water alone (Garcia 2001), leading to a gravitational instability. This instability leads to finger-like convection patterns, which greatly enhance the rate of dissolution of CO_2 into the medium. This process of fingering can lead to localization of the injected carbon dioxide and plays a dominant role in the long term.

One of the earliest analyses of the onset of convection in porous media was performed by Horton & Rogers Jr (1945) and Lapwood (1948) who dealt with the problem in isotropic media. This problem is characterized by a linear stationary base state in which stability can be characterized using a single non-dimensional parameter, the Rayleigh number. Convection occurs for all Rayleigh numbers greater than a critical value. For a given Rayleigh number, one can obtain the *critical wavenumber* corresponding to the length scale of the most unstable mode. The problem has been analysed using a linear stability approach similar to the one used for the clear fluid case (Chandrasekhar 1961). The predictions of the linear stability theory were found to be in good agreement with experiments as well as numerical simulations. The analysis was extended to anisotropic porous media by Castinel & Combarnous (1977) and Epherre (1977). An excellent discussion of the existing work is provided in the book by Nield & Bejan (1999).

The carbon sequestration problem is characterized by a time-dependent base state, and in this way differs from the problem studied by Horton & Rogers Jr (1945) and Lapwood (1948). The transient nature of the base state leads to the presence of a time scale (*critical time*) for the onset of convection along with the critical wavenumber. Caltagirone (1980) analysed the onset of convection using linear and energy stability analyses for the time-dependent problem with Dirichlet boundary conditions. Ennis-King & Paterson (2005) and Ennis-King, Preston & Paterson (2005) extended this analysis for an anisotropic porous medium, and obtained estimates for the critical time and the critical wavenumber. They also used single-term approximations of the Galerkin expansion to obtain analytic expressions for the dependence of critical time and wavenumbers on the anisotropy of the medium. Xu, Chen & Zhang

(2006) extended Ennis-King *et al.*'s work by considering the variation of both the horizontal and vertical permeabilities and found the dependence of critical time and wavenumbers on permeability to be simple power laws. Both of these sets of authors defined the critical time as the time required for the amplitude of the perturbations to begin amplifying. Following Ben, Demekhin & Chang (2002), Riaz *et al.* (2006) studied the problem for isotropic media using linear stability theory after a coordinate transformation to a similarity variable. They show that the solution resolves to the dominant mode rapidly in this formulation, allowing them to study the growth rate of just the dominant mode. They also conducted high-resolution numerical simulations and found good agreement for the growth rate of perturbations between the simulations and the stability theory. Kim, Kim & Kim (2004) and Park *et al.* (2006) studied the problem using propagation theory and Hassanzadeh, Pooladi-Darvish & Keith (2006) studied the linear stability using different initial conditions that span a range of wavenumbers.

The time-dependence of the base state causes considerable difficulty in analysing the linear stability of the system. When the governing PDEs are linearized and reduced to a set of coupled ODE–initial-value problems using a suitable eigenfunction expansion, the resulting matrix that combines the dynamics of various modes becomes time-dependent. The traditional approach of studying the eigenvalues is not applicable to general non-autonomous systems except for some special cases such as a periodic dependence where Floquet's theory can be applied (see Bauer & Nohel 1969). Further, the matrix is also not normal (i.e. does not commute with its adjoint) and therefore does not possess an orthogonal eigenvector-basis. Much progress has been made in the last decade in generalizing the traditional normal mode theory (applicable only when the matrix is normal) to the general non-normal non-autonomous case. This theory is called non-modal stability theory. An excellent description of the basic ideas can be obtained from Farrell & Ioannou (1996*a*,*b*) and the review article by Schmid (2007). Trefethen & Embree (2005) contains a detailed exposition on the very closely related idea of ϵ-pseudospectra along with many applications.

Linear stability analysis provides us with a sufficient condition for instability. The energy stability method, which is the nonlinear extension of the linear method, on the other hand provides us with a sufficient condition for stability. Here, one converts the PDEs for the evolution of the perturbation quantities into one for a suitably defined energy functional. Traditionally, the form of the energy functional used is a linear combination of the kinetic energy of the flow and the mean-squared magnitude of the perturbations. This equation is then analysed to obtain the conditions required for stability. These nonlinear (finite-amplitude) solutions may become unstable for many classes of problems which are linearly stable. So, the time scales obtained by energy analysis are lower than those obtained by linear stability analysis. Homsy (1973) studied the energy stability of impulsively heated fluid layers. A thorough description of the energy methods and their applications is provided by Straughan (2004).

While discussing the results of the linear stability analysis, Ennis-King *et al.* (2005) report two different problems with the approach that they used: (i) the choice of criterion for instability – due to linearization, the perturbations at any time t are always proportional to the initial perturbations, and there is no obvious choice of a critical time scale; and (ii) the choice of initial conditions – the 'white-noise' initial condition used is not localized within the diffuse zone as one would expect and need not correspond to the most unstable perturbation. In this work, we try to overcome these difficulties by applying the recently developed idea of non-modal stability theory.

We begin by briefly explaining the ideas of non-modal stability theory and present the approach used in this paper to analyse the growth of perturbations in our system. Compared to previous approaches, non-modal stability theory is a rigorously justified approach which provides the maximum amplification obtained among all possible perturbations at a given time. It also provides the structure of the initial perturbation which is most-amplified at any given time. After presenting the results obtained from the non-modal theory, we describe our three-dimensional, spectral numerical calculations and compare the growth rates predicted by non-modal theory to that measured from simulations. We find an excellent match between the simulations and the non-modal theory for very long times. Eventually, the perturbations amplify to such an extent that the nonlinear terms neglected in the linear theory become dominant. The above results suggest that the time at which nonlinear terms begin to dominate is an excellent, experimentally measurable indicator of the onset of convection.

The problem of subsurface flow in porous media is extremely complicated, and many research groups have been focusing much effort on methods of numerical simulation. Some of the most notable tools developed for modelling flow in porous media are the TOUGH2 code (Pruess 1991; Garcia 2003) developed at the Lawrence Berkeley Labs, the FEHM code (Zyvoloski *et al.* (http://fehm.lanl.gov/)) developed at the Los Alamos National Laboratory and the PFLOTRAN code (Lu & Lichtner 2005) also developed at Los Alamos.

2. Governing equations

In this paper, we only deal with the single-phase problem consisting of brine with dissolved carbon dioxide. The primary equations governing the flow are the same as those considered by Ennis-King *et al.* (2005) and Xu *et al.* (2006). They are Darcy's law for the momentum of the fluid, the advection diffusion equation for concentration of dissolved CO_2 and the continuity equation. Previous work (Garcia 2001) on the equation of state of the water–CO_2 system has shown that the dependence of the density of the medium on the concentration of CO_2 is approximately linear. Further, the maximum density difference between water saturated with CO_2 and pure water is only of the order of 1 %. So, we work in the framework of the Boussinesq approximation to simplify the problem. The governing equations are

$$\mu^* k^{*^{-1}} \boldsymbol{v}^* = -\nabla P^* + \rho_f^* g \boldsymbol{e}_z, \tag{2.1}$$

$$\phi \frac{\partial C^*}{\partial t^*} + \boldsymbol{v}^* \cdot \nabla^* C^* = \phi D^* \nabla^{*^2} C^*, \tag{2.2}$$

$$\nabla^* \cdot \boldsymbol{v}^* = 0, \tag{2.3}$$

$$\rho_f^* = \rho_0^*(1 + \beta C^*). \tag{2.4}$$

Here μ^* is the viscosity of the medium, k^* is the permeability of the medium, $\boldsymbol{v}^* = (u^*, v^*, w^*)$ is the Darcy velocity, C^* is the concentration of CO_2, P^* is the pressure, ρ_f^* is the density of the mixture, ϕ is the porosity, D^* is the diffusivity of CO_2 in water, ρ_0^* is the density of pure water, g is the acceleration due to gravity, β is the coefficient of volume expansion due to dissolution of CO_2 and $\boldsymbol{e}_z$ is the unit vector in the vertical direction. The asterisk denotes dimensional variables. The permeability field is assumed to be homogeneous and isotropic (constant everywhere). These equations are supplemented by the following boundary conditions for the vertical

velocity and the concentration of CO_2:

$$w^*(z^* = 0) = 0, \quad w^*(z^* = H^*) = 0,$$
$$C^*(z^* = 0) = C_0^*, \quad \frac{\partial C^*}{\partial z^*}(z^* = H^*) = 0,$$

where H^* is the depth of the domain. Recent two-phase simulations by Lindeberg & Bergmo (2003) have shown that the interface between supercritical CO_2 and brine remains flat. The concentration of dissolved CO_2 in the immediate vicinity of the interface is modelled as a constant, C_0. Following Xu *et al.* (2006) and Ennis-King *et al.* (2005), we non-dimensionalize the above equations with the following reference variables:

$$X = H^*, \quad T = \frac{H^{*2}}{D^*},$$
$$V = \frac{\phi D^*}{H^*}, \quad P = \frac{\mu^* \phi D^*}{k^*},$$
$$C = C_0^*.$$

The non-dimensional equations which are obtained are

$$\boldsymbol{v} = -\nabla P + RaC\boldsymbol{e}_z, \tag{2.5}$$

$$\frac{\partial C}{\partial t} + \boldsymbol{v} \cdot \nabla C = \nabla^2 C, \tag{2.6}$$

$$\nabla \cdot \boldsymbol{v} = 0, \tag{2.7}$$

$$C(z = 0) = 1, \quad \frac{\partial C}{\partial z}(z = 1) = 0, \tag{2.8}$$

$$w(z = 0) = 0, \quad w(z = 1) = 0, \tag{2.9}$$

where Ra is the Rayleigh number defined as

$$Ra = \frac{k^* \rho_0^* \beta C_0^* g H^*}{\mu^* \phi D^*}.$$

By taking divergence of the momentum equation, we obtain a Poisson equation for pressure:

$$\nabla^2 P = Ra \frac{\partial C}{\partial z}. \tag{2.10}$$

This equation can be used to eliminate pressure from the vertical momentum equation, resulting in

$$\nabla^2 w = Ra \left(\frac{\partial^2 C}{\partial x^2} + \frac{\partial^2 C}{\partial y^2} \right). \tag{2.11}$$

We formally separate the concentration and the pressure into their base state and wave-like-perturbations with a fixed horizontal wavenumber $\boldsymbol{k} = (k_x, k_y)$:

$$C = C_{ref} + \epsilon\theta, \quad P = P_{ref} + \epsilon\Pi,$$
$$\theta = \sum_n \hat{\theta}_n(t) \, e^{i\boldsymbol{k}\cdot\boldsymbol{x}} \sin\left(\left(n - \frac{1}{2}\right)\pi z\right),$$
$$w = \sum_n \hat{w}_n(t) \, e^{i\boldsymbol{k}\cdot\boldsymbol{x}} \sin(n\pi z).$$

Here, C_{ref} and P_{ref} are the base states of concentration and pressure respectively, θ and Π are the perturbations and ϵ is a measure of the amplitude of initial perturbations. In the above equations, the eigenfunctions in the vertical direction are chosen to satisfy the boundary conditions (2.8)–(2.9).

Substituting this decomposition into the governing equations, we see that the base-state equation is the diffusion equation:

$$\frac{\partial C_{ref}}{\partial t} = \frac{\partial^2 C_{ref}}{\partial z^2}, \qquad (2.12)$$

$$C_{ref}(z = 0) = 1, \qquad \frac{\partial C_{ref}}{\partial z}(z = 1) = 0. \qquad (2.13)$$

The analytical solution of the base state is given by

$$C_{ref}(z, t) = 1 - \frac{4}{\pi} \sum_n \frac{1}{2n - 1} \, e^{-(n-1/2)^2 \pi^2 t} \, \sin\left(\left(n - \frac{1}{2}\right) \pi z\right). \qquad (2.14)$$

The perturbation equations are

$$\boldsymbol{v} = -\nabla \Pi + Ra\theta \boldsymbol{e}_z,$$

$$\frac{\partial \theta}{\partial t} + w \frac{\mathrm{d} C_{ref}}{\mathrm{d} z} = \nabla^2 \theta - \epsilon \boldsymbol{v} \cdot \nabla \theta,$$

$$\theta(z = 0) = 0, \qquad \frac{\partial \theta}{\partial z}(z = 1) = 0,$$

$$w(z = 0) = 0, \qquad w(z = 1) = 0.$$

The equations governing the linear growth of perturbations are obtained by neglecting the $O(\epsilon)$ term in this set of equations. After neglecting the nonlinear term and using the eigenfunction expansion for θ and w, we can reduce the above set of PDEs to a coupled set of ODE–initial-value problems:

$$\frac{\mathrm{d}}{\mathrm{d} t} \hat{\theta}_n = G_{nm} \hat{\theta}_m, \qquad (2.15)$$

$$\boldsymbol{G} = \boldsymbol{A}^{-1} [\boldsymbol{B} - Ra_h \boldsymbol{C} \boldsymbol{E}^{-1} \boldsymbol{D}], \qquad (2.16)$$

$$A_{nm} = \frac{1}{2} \delta_{nm}, \qquad (2.17)$$

$$B_{nm} = -\frac{1}{2} \left[k^2 + \left(m - \frac{1}{2}\right)^2 \pi^2 \right] \delta_{nm}, \qquad (2.18)$$

$$C_{nm} = -\frac{1}{2} \left[\exp\left\{ -\left(m + n - \frac{1}{2}\right)^2 \pi^2 t \right\} - \exp\left\{ -\left(m - n + \frac{1}{2}\right)^2 \pi^2 t \right\} \right], \qquad (2.19)$$

$$D_{nm} = (-1)^{n+m} \frac{s^2 n}{\pi \left(n + m - \frac{1}{2}\right) \left(n - m + \frac{1}{2}\right)}, \qquad (2.20)$$

$$E_{nm} = -\frac{1}{2} (k^2 + m^2 \pi^2) \delta_{nm}. \qquad (2.21)$$

The time-dependence of the matrix $\boldsymbol{G}$ has caused some problems in analysing the stability of the system. Previous researchers have either used a quasi-steady-state approximation (QSSA) (Rogers & Morrison 1950) where the matrix is held fixed at some instant of time t_0 or have solved the initial-value problem with arbitrary initial conditions. QSSA assumes a separation in time scales where the growth rate of

perturbations is much larger than the rate of change of the base state. Tan & Homsy (1986) compared the QSSA approach to the solution of the initial-value problem to study the onset of viscous fingering and found that the solution of the initial-value problem was more accurate than the QSSA at early time and the two methods give similar results at large times.

In the second approach the initial-value problem is solved with a so-called 'white-noise' initial condition, for which the perturbation is specified as $\hat{\theta}_n = 1$ for all n. This initial condition was found by Foster (1965) to give the fastest growth rate of perturbations and was obtained by choosing the fastest observed critical time among a finite number of trials. It has been recognized (Ennis-King *et al.* 2005) that there are at least two problems with this approach. First, the initial condition chosen might not necessarily correspond to the one giving the fastest growth of perturbations. In principle, one is interested in the perturbations which are most amplified at any given time. So far, it has been difficult to determine these most-amplified initial perturbations. Further, the white-noise condition perturbs the system everywhere, while one would expect the perturbations to be localized in the diffusive zone. Second, there is no obvious way of defining a critical time for the onset of instability. The amplitude of the perturbations decays at early time due to the action of diffusion. At later times, the amplitude of the perturbations begins to grow and convection is expected to be the dominant phenomena. For this reason, Xu *et al.* (2006) and Ennis-King *et al.* (2005) used the following criterion as the definition of the critical time:

$$\frac{\mathrm{d}}{\mathrm{d}t} \left(\int \theta^2 \mathrm{d}x \right)_{t=t_c} = 0. \tag{2.22}$$

3. Non-modal stability theory

In this section, we give a brief description of the non-modal stability theory. For the sake of brevity, only the basic idea is presented. Equations (2.15)–(2.21) can be concisely written in vector notation as:

$$\frac{\mathrm{d}}{\mathrm{d}t} \boldsymbol{x} = \boldsymbol{G}\boldsymbol{x},$$

where $\boldsymbol{x}$ is the vector of coefficients $\hat{\theta}_n$. To maintain clarity, we first discuss the idea of non-modal stability for a matrix $\boldsymbol{G}$ which has no time-dependence and then generalize the discussion to the non-autonomous case. If the matrix $\boldsymbol{G}$ has no time-dependence, the formal solution is given by

$$\boldsymbol{x}(t) = \mathrm{e}^{\boldsymbol{G}t} \boldsymbol{x}(0)$$

where $\mathrm{e}^{\boldsymbol{G}t}$ is the familiar matrix exponential. Now diagonalizing $\boldsymbol{G}$ as $\boldsymbol{G} = \boldsymbol{V}\boldsymbol{\Lambda}\boldsymbol{V}^{-1}$, we obtain the following for the amplification σ:

$$\sigma(t) = \max_{\boldsymbol{x}_0} \frac{||\boldsymbol{x}(t)||}{||\boldsymbol{x}(0)||} = ||\boldsymbol{V}\mathrm{e}^{\boldsymbol{\Lambda}t}\boldsymbol{V}^{-1}||,$$

where the norm of a vector is the typical Euclidean norm and the norm of a matrix is taken to be the induced norm defined as

$$||\boldsymbol{G}|| = \max_{||\boldsymbol{x}||=1} ||\boldsymbol{G}\boldsymbol{x}||. \tag{3.1}$$

If the matrix $\mathbf{G}$ is a normal matrix, then it has an orthogonal set of eigenvectors and $\mathbf{V}$ is a unitary matrix. In this special case, we recover the normal mode theory $\sigma = e^{\lambda_{max}t}$. However, if $\mathbf{G}$ is not a normal matrix, the growth of perturbations is not given by the eigenvalues alone and one has to consider the entire norm $||\mathbf{V}e^{\Lambda t}\mathbf{V}^{-1}||$. For a non-normal matrix $\mathbf{G}$, the eigenvalues only describe the dynamics of the system in the asymptotic limit as $t \to \infty$. However, what one is most interested in is the finite-time amplification of perturbations. When the eigenvectors are not orthogonal to each other, one can form combinations of these eigenvectors which amplify temporarily, even if all the eigenvectors are characterized by negative eigenvalues. This finite-time growth can amplify the perturbations to such an extent that the nonlinear terms neglected in the analysis ($\mathbf{v} \cdot \nabla\theta$) are no longer negligible. A comprehensive account of non-modal stability theory is presented in Farrell & Ioannou (1996*a*) and a recent text on the subject with applications to shear flow is Schmid & Henningson (2001). For a recent review on the subject, refer to Schmid (2007).

To compute the norm of the matrix $e^{\mathbf{G}t}$, the idea of singular-value decomposition (SVD) is used (see Golub & Loan 1996). SVD is a generalization of the idea of eigenvalues to non-normal (even non-square) matrices. The matrix $e^{\mathbf{G}t}$ can be written as

$$e^{\mathbf{G}t} = \mathbf{U}\Sigma\mathbf{V}^{T}, \tag{3.2}$$

where Σ is a diagonal matrix of the singular values of $e^{\mathbf{G}t}$. The growth of perturbations is bounded by the largest singular value. The matrices $\mathbf{U}$ and $\mathbf{V}$ are orthogonal matrices and it can be shown that the column of $\mathbf{V}$ corresponding to the largest singular value is the most amplified initial vector, whose final state is the corresponding column of $\mathbf{U}$.

In the case of non-autonomous systems

$$\frac{d}{dt}x = \mathbf{G}(t)x, \tag{3.3}$$

the analysis is slightly modified as the matrix exponential is no longer the fundamental solution. Let us define the fundamental solution operator (or the propagator) of the system as

$$x(t) = \mathbf{X}(t;t_0)x(t_0), \tag{3.4}$$

i.e. $\mathbf{X}(t;t_0)$ is a time-dependent matrix that transforms any initial condition at time t_0 into the solution of the initial-value problem at time t. Substituting (3.4) into (2.15)–(2.21), we obtain the following matrix differential equation:

$$\frac{d}{dt}\mathbf{X}(t;t_0) = \mathbf{G}(t)\mathbf{X}(t;t_0), \tag{3.5}$$

with the initial condition,

$$\mathbf{X}(t_0;t_0) = \mathbf{I}, \tag{3.6}$$

where $\mathbf{I}$ is the identity matrix. This is now a well-posed problem with known initial conditions. The solution of this differential equation effectively solves the linear system in (3.3) for the entire space of initial conditions. Now, the amplification can be computed from

$$\sigma(t) = \max_{x_0} \frac{||x(t)||}{||x(t_0)||} = ||\mathbf{X}(t;t_0)||. \tag{3.7}$$
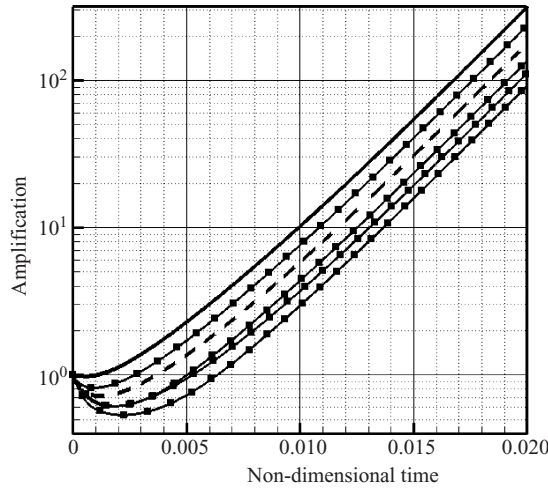
FIGURE 2. Amplification predicted from non-modal theory (solid line) compared to that obtained using the solution of the ODE with random initial perturbations (lines with symbols – four different realizations are shown). The initial condition used by Ennis-King *et al.* (2005) and Xu *et al.* (2006) is also shown (dashed line).

This is the approach that is followed in this paper. We use a fourth-order Runge–Kutta method to solve the initial-value problem in (3.5) for the fundamental solution operator $\boldsymbol{X}(t;t_0)$. Then a singular-value decomposition of this matrix gives us the largest growth possible for any initial condition, along with the initial condition that leads to this growth. In figure 2, we compare the amplification of perturbations obtained using the non-modal stability theory (solid line) to the growth rate obtained from the solution of the initial-value problem where the initial conditions were generated using a random number generator for $Ra = 400$, $k = 3\pi$. The growth predicted from the initial condition used by Ennis-King *et al.* (2005) and Xu *et al.* (2006) is also shown (dashed line). The critical time is defined by these authors as the minimum in the amplification curve (at $t \sim 0.001$). The growth calculated from the non-modal theory is the maximum among all possible initial conditions, and one can obtain the initial condition which realizes this growth using a singular-value decomposition as described above.

In figure 3, we show the maximum amplification achieved by the perturbations as a function of the horizontal wavenumber of the initial perturbation. The system has a Rayleigh number of $Ra = 100$. It can be seen that in the limit $t \to \infty$, the perturbations of all wavenumbers decay. However, they can undergo significant amplification (about 4 orders of magnitude) in a finite amount of time, even for a rather low Rayleigh number of 100. If during this period of amplification the neglected nonlinear terms $(\boldsymbol{v} \cdot \nabla\theta)$ become so large that they cannot be neglected any more, the linear theory is no longer applicable and the dynamics of the perturbations take a different route from that suggested by linear theory. The wavenumber achieving maximum amplification is seen to be $k = 4.1888$ and the corresponding wavelength is $1.5H^*$.

Non-modal stability theory also provides us with the structure of the most amplified perturbation. It can be seen from figure 3 that, among the wavenumbers shown, at $t = 0.6$ the most amplified wavenumber is $|k| = 4.1888$ whereas at $t = 1.5$, the most amplified wavenumber is $|k| = 2.9322$. In figure 4, we show the most amplified
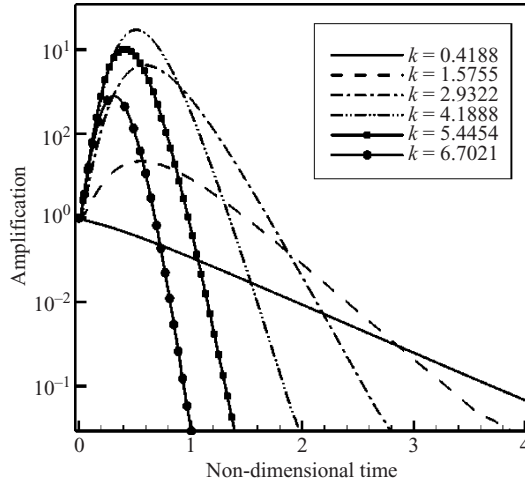
FIGURE 3. Effect of wavenumber of perturbation on the maximum amplification achieved for $Ra = 100$. The dominant wavenumber is different at different times.
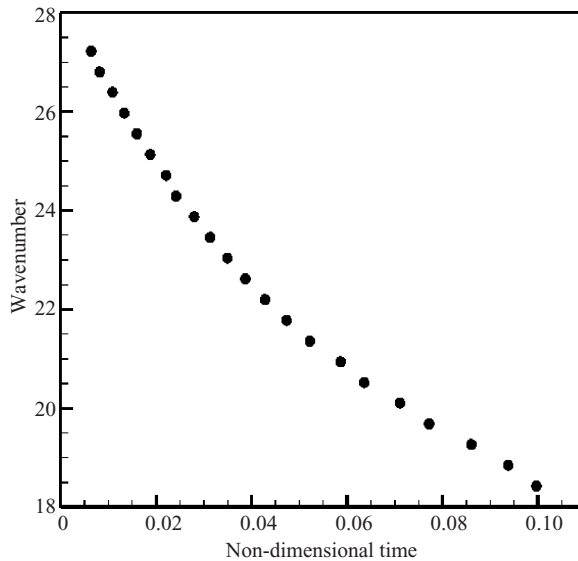
FIGURE 4. Horizontal wavenumber of the most amplified initial perturbation at different times for $Ra = 1000$.

wavenumber as a function of the non-dimensional time for $Ra = 1000$. The non-modal calculations were performed for a series of wavenumbers, and at each time we plot the wavenumber which achieves the most amplification. We see that at early times large wavenumbers are excited leading to a small-scale structure of the flow field. At later times, the long-wave perturbations are most active. At the onset of fingering, we expect to see a range of wavenumbers, each amplified according to the corresponding growth predicted from theory. In figure 5, we show the contours of the initial perturbation of concentration that is most amplified at $t = 0.01$. As expected, we see that the perturbation is localized within the diffusive zone. Owing to the spatial symmetry of the governing equations in the horizontal direction, we
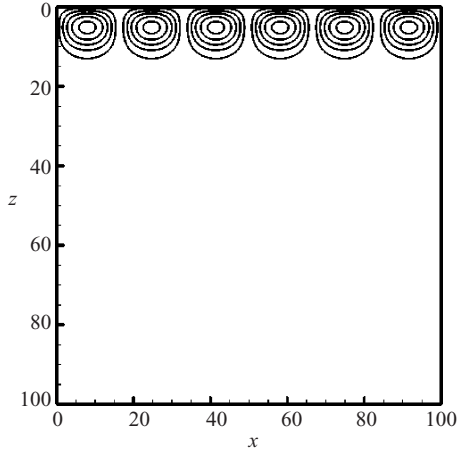
FIGURE 5. Contours of the most unstable initial perturbation for $Ra = 1000$.

can only obtain the magnitude of the wavenumber vector $|k| = (k_x^2 + k_y^2)^{1/2}$. It is not possible to predict which combination of k_x and k_y will be realized in practice. For the contours of concentration shown in figure 5, we have taken $k_x = k_y = |k|/\sqrt{2}$.

4. Direct numerical simulations

4.1. *Description of the numerical method*

In this section, we describe the three-dimensional pseudo-spectral direct numerical simulations of the governing equations. Looking at the eigenfunction expansion of the base state in (2.14), we see that the coefficients of the expansion decay super-exponentially at any finite time. This implies that a numerical simulation utilizing these eigenfunctions will demonstrate spectral accuracy. This rapid convergence can be expected to hold as long as the diffusive state has some dominance in the dynamics of the system. At later times, when the nonlinear convection process becomes dominant, the accuracy need not necessarily be exponential; however it is still much more accurate than any traditional finite-volume method. Further, at $t \sim 0$, the coefficients only decay as $\hat{\theta}_n \sim n^{-1}$ leading to bad convergence properties. For this reason, all the numerical simulations performed use an initial condition given by the base-state profile (2.14) at a finite time $t = 0.001$. This corresponds to letting the system diffuse for some time, before the perturbations are added. An excellent introduction to the pseudospectral method and considerations of its accuracy are provided in the books by Canuto *et al.* (1988) and Peyret (2002).

Given the concentration field at any discrete time $C^{(n)}(\boldsymbol{x}) = C(t^{(n)}, \boldsymbol{x})$, we need to calculate the velocity field in order to advance to the next time step. In our formulation, we first solve the Poisson equation for the vertical velocity (2.11) for w. We now need two more equations to solve for the horizontal components of velocity. One of these equations is the constraint of incompressibility:

$$\frac{\partial u}{\partial x} + \frac{\partial v}{\partial y} = -\frac{\partial w}{\partial z}. \tag{4.1}$$

The second equation is obtained by taking a curl of Darcy's equation, to obtain an equation for the vorticity:

$$\omega = \frac{\partial C}{\partial y}\boldsymbol{e}_x - \frac{\partial C}{\partial x}\boldsymbol{e}_y. \tag{4.2}$$

In particular, for the vertical component of the vorticity, we have

$$\omega_z = \frac{\partial v}{\partial x} - \frac{\partial u}{\partial y} = 0. \tag{4.3}$$

Once the vertical component of the velocity is obtained, the horizontal components are obtained by solving (4.1) and (4.3) simultaneously.

The spectral method used in this work expands the concentration and vertical velocity using Fourier-modes in the horizontal direction and the relevant eigenfunctions in the vertical direction:

$$C = \sum_{k,n} \widehat{C}_{kn} e^{i k \cdot x} \sin\left(\left(n - \frac{1}{2}\right)\pi z\right), \tag{4.4}$$

$$w = \sum_{k,n} \widehat{w}_{kn} e^{i k \cdot x} \sin\left(n\pi z\right), \tag{4.5}$$

$$u = \sum_{k} \widehat{u}_k(z) e^{i k \cdot x}, \tag{4.6}$$

$$v = \sum_{k} \widehat{v}_k(z) e^{i k \cdot x}, \tag{4.7}$$

where $k = (k_x, k_y)$ are the wavenumbers of the perturbations in the horizontal directions and $\widehat{C}_{kn}, \widehat{w}_{kn}, \widehat{u}_{kn}$ and $\widehat{v}_{kn}$ are the coefficients of the eigenfunction expansion. Using the above expansions in (2.11) along with the orthogonality of the eigenfunctions, we obtain

$$\widehat{w}_{km} = \frac{2Rak^2}{k^2 + m^2\pi^2} W_{mn}\widehat{C}_{kn} \tag{4.8}$$

where $\boldsymbol{W}$ is a matrix of inner-products of the various eigenfunctions of w and C,

$$W_{mn} = \int_0^1 \sin(m\pi z)\sin\left(\left(n - \frac{1}{2}\right)\pi z\right)\mathrm{d}z$$

$$= \frac{(-1)^{(m+n)}m}{\pi\left(m - n + \frac{1}{2}\right)\left(m + n - \frac{1}{2}\right)}.$$

For every wavenumber k, the above operation gives the spectral coefficients of the vertical velocity component using a simple matrix-vector multiplication. Now using (4.5)–(4.7) in (4.1) and (4.3), the horizontal components of the velocity can be obtained for each wavenumber as

$$\widehat{u}_k(z) = \frac{i k_x}{k^2}\frac{\partial \widehat{w}_k}{\partial z}, \tag{4.9}$$

$$\widehat{v}_k(z) = \frac{i k_y}{k^2}\frac{\partial \widehat{w}_k}{\partial z} \tag{4.10}$$

where

$$\hat{w}_k(z) = \sum_{n} \hat{w}_{kn} \sin\left(n\pi z\right). \tag{4.11}$$
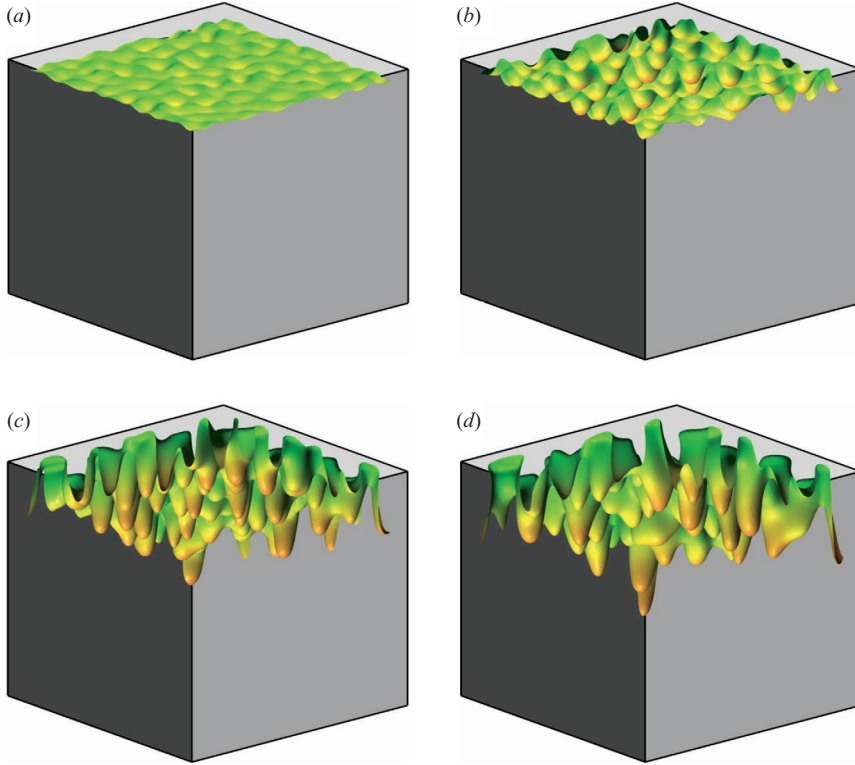
FIGURE 6. Isosurfaces of the concentration of carbon dioxide for a simulation with $Ra = 1000$. The isosurfaces are plotted at (a) $t = 1.59 \times 10^{-3}$, (b) $t = 2 \times 10^{-3}$, (c) $t = 3 \times 10^{-3}$ and (d) $t = 4 \times 10^{-3}$.

Once the Fourier-transformed velocity fields have been computed slice-by-slice, the velocity in the physical space can be obtained by a fast Fourier transform operation. The nonlinear term is calculated using the pseudospectral technique in physical space. The transport equation is advanced in time using a second-order Runge–Kutta method. The simulations are carried out using a non-dimensional time step of 10^{-6} and a grid resolution of 128^3. For a domain depth of 40 m, this corresponds to a physical time step of 18.5 days and a grid spacing of 0.3 m. The simulation is parallelized along slices in the horizontal direction. Using 16 processors, the simulations take about one hour for every 1000 time steps. A simple diffusion test was conducted where the initial condition was the base-state profile at $t_0 = 0.001$. The error between the numerical simulation and the analytical result for the concentration field at all subsequent times was of $O(\Delta t^2)$ and the velocity field was exactly $\boldsymbol{v} = \boldsymbol{0}$. In figure 6, we show isosurfaces of the concentration of carbon dioxide ($C = 0.3$) at different times, obtained using the spectral simulations. The Rayleigh number for these plots is $Ra = 1000$. The simulations were also performed with various combinations of k_x and k_y of initial perturbation keeping $|k|$ fixed. As predicted by the linear theory, the amplifications for these different cases only depends on $|k|$ and not on the values of k_x and k_y.

4.2. *Comparison with non-modal stability theory*

The most unstable perturbation extracted from the non-modal stability theory was given as the initial condition for the three-dimensional simulations. Using the
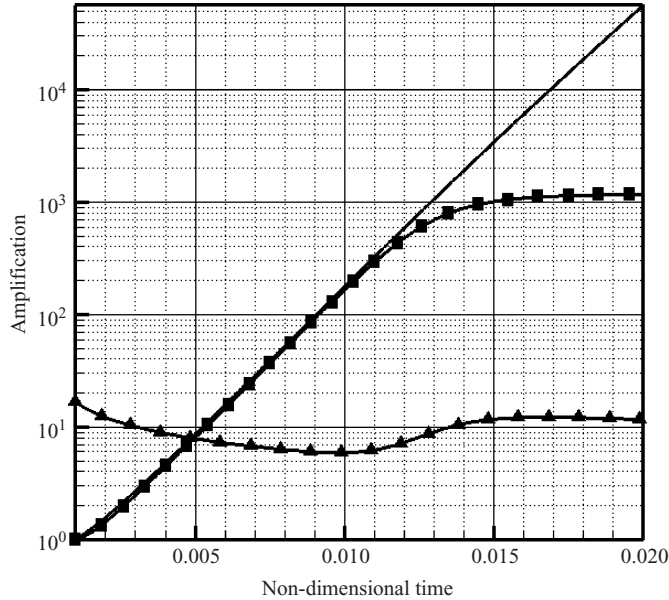
FIGURE 7. Comparison of the amplifications from non-modal theory (solid line) and simulations (squares). Also plotted is the total dissolution flux (triangles).

analytical solution for the base state, the amplification of perturbations was computed at every time step using

$$\sigma^{(n)}(t) = \int \left(C^{(n)}(\boldsymbol{x}) - C_{ref}(z, t^n) \right)^2 \mathrm{d}\boldsymbol{x}$$

In figure 7, we show the amplification predicted by the linear theory using a solid line and that measured in the simulations using squares. The parameters for the test are $Ra = 400$ where the initial perturbation is with wavenumber $\boldsymbol{k} = (4\pi, 2\pi)$. It can be seen that there is an excellent match between the theory and simulations up to $t = 0.01$ when the growth of perturbations in the simulations slowly begins to saturate. This saturation occurs when the nonlinear term $\boldsymbol{v} \cdot \nabla\theta$, which was neglected in deriving the linear ODEs, becomes large enough that it cannot be neglected any more. Beyond this time, the linear theory is no longer valid and the amplification predicted by the theory is not a meaningful quantity.

As has already been noted by Ennis-King *et al.* (2005), the process of linearization makes it difficult to define a time scale for the onset of convection. Looking at the amplification curve obtained from non-modal theory in figure 7, it is clear that there is no natural way of picking a characteristic time scale which we can define as the onset of convection. Further, we can rigorously prove that the linear problem is asymptotically stable (refer to Bauer & Nohel 1969). This is a consequence of the finite size of the domain where all the perturbations eventually have to diminish (in the $t \to \infty$ limit). In this paper, we claim that the time at which the nonlinear terms begin to dominate is a useful characteristic time scale for the problem.

Since the reason we are interested in the fingering process is enhancement of dissolution, let us consider the total rate of dissolution of carbon dioxide into the

saline aquifer. Integrating the transport equation, we obtain the following equation:

$$\frac{\mathrm{d}}{\mathrm{d}t} \int C \mathrm{d}x = \int (\nabla C \cdot n)_{z=0} \, \mathrm{d}S. \tag{4.12}$$

The integral on the right is the total instantaneous flux of dissolution into the system, J, which can be written as the sum of contributions from the base state and the perturbations:

$$\begin{aligned} J &= -\left(\frac{\partial C}{\partial z}\right)_{z=0} \\ &= -\left(\frac{\partial C_{ref}}{\partial z}\right)_{z=0} - \epsilon \left(\frac{\partial \theta}{\partial z}\right)_{z=0}. \end{aligned} \tag{4.13}$$

The flux due to the base state can be computed explicitly as

$$-\left(\frac{\partial C_{ref}}{\partial z}\right)_{z=0} = 2 \sum_n \mathrm{e}^{-(n-1/2)^2 \pi^2 t}. \tag{4.14}$$

Taking a time-derivative to compute the rate at which the total flux is changing, we obtain

$$\frac{\mathrm{d}}{\mathrm{d}t} J = -2 \sum_n \left(n - \frac{1}{2}\right)^2 \pi^2 \mathrm{e}^{-(n-1/2)^2 \pi^2 t} + \epsilon \frac{\mathrm{d}}{\mathrm{d}t} \left[-\left(\frac{\partial \theta}{\partial z}\right)_{z=0}\right]. \tag{4.15}$$

In this equation, the first term on the right is the contribution due to the base state. This term is always negative, since diffusion tends to reduce the gradients of concentration. The second term is the contribution of the perturbations, and is positive or negative depending on whether the perturbations are being damped by diffusion, or are increasing owing to the amplification of perturbations.

When the perturbations are small enough that the linear theory is still valid, we have

$$\left(\frac{\partial \theta}{\partial z}\right)_{z=0} = \sum_k \left(n - \frac{1}{2}\right) \pi \hat{\theta}_{kn} \mathrm{e}^{\mathrm{i}k \cdot x}.$$

The perturbations do not make any contribution to the total flux owing to their wave-like nature. Within the limits of linear theory, the flux is entirely due to the base state. Once the perturbations amplify sufficiently that the linear theory does not hold any more, the total flux begins to rise sharply. In figure 7, we have also plotted the total dissolution flux measured from the simulation (plotted using triangles). We can see that, as the growth of perturbations begins to deviate from the predictions of the non-modal theory, the total flux begins to rise sharply. The time at which the total flux reaches a minimum and begins to amplify corresponds very closely to the time at which the amplification of the perturbations from the spectral simulations begins to deviate from the linear theory. After this, the total flux begins to rise sharply and this is the time when the fingers are growing rapidly. In the results of the spectral simulation shown in figure 6, the isosurfaces shown in (*a*) correspond to the time at which the total flux has reached a minimum. One can see the formation of the early fingers which grow rapidly in figure 6(*b–d*).

We claim that for homogeneous systems the time at which the total dissolution flux begins to increase is a useful characteristic time scale of the problem, and that this time corresponds to the birth of the fingers. We define the time for the onset of
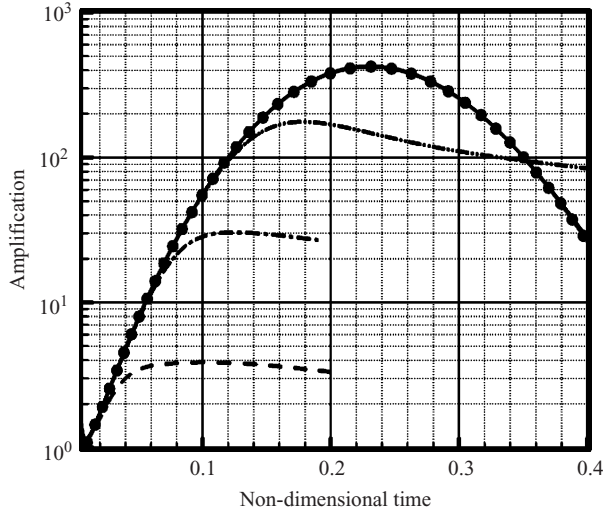
FIGURE 8. Evolution of the total flux at the top boundary for different amplitudes of initial perturbation. The bold circles are predictions from the non-modal theory and the various lines are: dashed: $\epsilon = 10^{-1}$, dash-dot: $\epsilon = 10^{-2}$, dash-dot-dot: $\epsilon = 10^{-3}$ and bold solid line: $\epsilon = 10^{-5}$.

convection as

$$\left(\frac{\mathrm{d}}{\mathrm{d}t}J\right)_{t=t_{onset}} = 0. \tag{4.16}$$

Foster (1965) mentions that 'At some point during this superexponential growth the disturbance will grow so rapidly that it will cause the fluid to rather suddenly appear to exhibit 'instability'. It seems reasonable to assume that this 'onset of instability' will be manifest when the averaged velocity disturbance has increased by a factor between one and three orders of magnitude'. We believe that this sudden appearance of instability occurs when the nonlinear terms have undergone sufficient amplification that the total flux begins to increase.

   We now consider the effect of varying the amplitude of the initial perturbation. In figure 8, we plot the evolution of the total flux at the top of the boundary for four different simulations with a Rayleigh number of $Ra = 120$ and $(k_x, k_y) = (2\pi, 2\pi)$. These simulations were carried out with the same initial condition, but with magnitudes of perturbation strength ϵ of 10^{-1} (dashed line), 10^{-2} (dash-dot), 10^{-3} (dash-dot-dot) and 10^{-5} (solid line). The symbols correspond to the growth rate predicted by the non-modal theory. It can be seen that as the perturbation is made weaker, the time at which the nonlinear terms begin to dominate increases. For this example with a relatively low Rayleigh number, when the perturbation strength is $\epsilon = 10^{-5}$, the nonlinear term never becomes dominant. For a real physical system, it is difficult to characterize the amplitude of initial perturbations. Real systems are always heterogeneous and contain variations in the permeability field at all length scales. These variations in the permeability field provide us with the perturbations which eventually lead to the formation of fingers. One can reason that the amplitude of perturbations can be related to some measure of the magnitude of fluctuations of the permeability field within the diffuse layer. Further work is required to understand and quantify this dependence.

5. Discussion

In this paper, we have used non-modal stability theory to rigorously obtain the maximum growth rate achieved by any perturbation at a given time. To the best of our knowledge, such an approach has not yet been applied to study stability of flows in porous media. We have also used this approach to derive the spatial structure of the initial perturbations which lead to this growth. The most-amplified initial perturbations are seen to be strongly localized within the diffusive zone as one would expect. This is a significant improvement on previous results which had to depend on solutions of an initial-value problem with arbitrary initial conditions where the perturbations are distributed over all space. We have also developed an extremely accurate three-dimensional spectral solver for the governing equations and shown that the growth rates predicted from theory match extremely well with those observed in simulation.

As shown in the previous Section, the time at which the perturbations saturate (and the process of convection begins) is strongly related to the strength of the initial perturbations. In a real physical system, the perturbations are introduced by the heterogeneous nature of the porous medium. Real porous media are heterogeneous over a very wide range of length scales, leading to a continuous perturbation over many different scales. Engineering simulations, however, filter out a large spectrum of these perturbations due to a shortage of experimental data. The simulations presented in this paper are a limiting case of such a filtering process, whereby all the perturbations of the porous medium are eliminated to yield a homogeneous system and the effects of those perturbations have been modelled by the initial perturbations added to the system. As seen from the results of the previous Sections (and from preliminary simulations with fully heterogeneous media, to be presented elsewhere), the exact nature and magnitude of perturbations plays a significant role in the dynamics of the system. So, we can see that the amplitude of initial perturbations is a parameter that needs to be obtained before we can make predictions of the time scales of convection at a given site. The amplitude of initial perturbations can in principle be obtained experimentally by computing the heat flux in a core-scale thermal experiment and comparing it to numerical simulations. With the knowledge of the effective magnitude of initial perturbations, we will be in a position to make predictions of the time scales of convection. Studies of the onset of convection in heterogeneous media are rather limited. A stochastic study of the effect of heterogeneity on the onset of convection is given in Prasad & Simmons (2003). Further research is needed in this direction to quantify the effects of the heterogeneity of the medium.

The purpose of these simulations is to provide valuable insight into the roles of various parameters in the process of the onset of convection and not to provide long-time results for the problem. Additional effects that need to be considered in the future are capillary effects, and those of reaction and dispersion. For reasons of simplicity, we have also assumed one of the principal axes of the permeability tensor to be aligned with the direction of gravity. The effects of the orientation of the porous media also need to be considered in the future.

REFERENCES

BAUER, F. & NOHEL, J. A. 1969 *The Qualitative Theory of Ordinary Differential Equations: An Introduction*. Dover.

BEN, Y., DEMEKHIN, E. A. & CHANG, H.-C. 2002 A spectral theory for small-amplitude miscible fingering. *Phys. Fluids* **14** (3), 999–1010.

CALTAGIRONE, J.-P. 1980 Stability of a saturated porous layer subject to a sudden rise in surface temperature: comparison between the linear and energy methods. *Q. J. Mech. Appl. Maths* **3**, 47–58.

CANUTO, C., HUSSAINI, M. Y., QUARTERONI, A. & ZANG, T. A. 1988 *Spectral Methods in Fluid Dynamics*. Springer.

CASTINELL, G. & COMBARNOUS, M. 1977 Natural convection in an anisotropic porous medium. *Intl Chem. Engng* **17**, 605–613.

CHANDRASEKHAR, S. 1961 *Hydrodynamic and Hydromagnetic Stability*. Clarendon.

ENNIS-KING, J. & PATERSON, L. 2005 Role of convective mixing in the long-term storage of carbon dioxide in deep saline formations. *SPE J.* **10**, 349–356.

ENNIS-KING, J., PRESTON, I. & PATERSON, L. 2005 Onset of convection in anisotropic porous media subject to a rapid change in boundary conditions. *Phys. Fluids* **17** (8), 084107.

EPHERRE, J. F. 1977 Criterion for the appearance of natural convection in an anisotropic porous layer. *Intl Chem. Engng* **17**, 615–616.

FARRELL, B. F. & IOANNOU, P. J. 1996a Generalized stability theory. part i: Autonomous operators. *J. Atmos. Sci.* **53** (14), 2025–2040.

FARRELL, B. F. & IOANNOU, P. J. 1996b Generalized stability theory. part ii: Nonautonomous operators. *J. Atmos. Sci.* **53** (14), 2041–2053.

FOSTER, T. D. 1965 Stability of a homogeneous fluid cooled uniformly from above. *Phys. Fluids* **8** (7), 1249–1257.

GARCIA, J. E. 2001 Density of aqueous solutions of CO_2. *Tech. Rep.* LBNL-49023. Lawrence Berkeley National Laboratory.

GARCIA, J. E. 2003 Fluid dynamics of carbon dioxide disposal into saline aquifers. PhD thesis, University of California, Berkeley.

GOLUB, G. H. & VAN LOAN, C. F. 1996 *Matrix Computations*. The Johns Hopkins University Press.

HASSANZADEH, H., POOLADI-DARVISH, M. & KEITH, D. W. 2006 Stability of a fluid in a horizontal saturated porous layer: effect of non-linear concentration profile, initial, and boundary conditions. *Transport in Porous Media* **65** (2), 193–211.

HOMSY, G. M. 1973 Global stability of time-dependent flows: impulsively heated or cooled fluid layers. *J. Fluid Mech.* **60** (1), 129–139.

HORTON, C. W. & ROGERS JR, F. T. 1945 Convection currents in a porous media. *J. Appl. Phys.* **16**, 367–370.

IPCC 2005 *IPCC Special Report on Carbon Dioxide Capture and Storage*. Prepared by Working Group III of the Intergovernmental Panel on Climate Change (B. Metz, O. Davidson, H. C. de Coninck, M. Loos and L. A. Meyer). Cambridge University Press.

KIM, M. C., KIM, K. Y. & KIM, S. 2004 The onset of transient convection in fluid-saturated porous layer heated uniformly from below. *Int. Comm. Heat Mass Transfer* **31** (1), 53–62.

LAPWOOD, E. R. 1948 Convection of a fluid in a porous medium. *Proc. Camb. Phil. Soc.* **44**, 508–521.

LINDEBERG, E. & BERGMO, P. 2003 The long-term fate of CO_2 injected into an aquifer. In *Greenhouse Gas Control Technologies* (ed. J. Gale & Y. Kaya), vol. 1, pp. 489–495. Elsevier.

LU, C. & LICHTNER, P. C. 2005 PFLOTRAN: Massively parallel 3-D simulator for CO_2 sequestration in geologic media. *Fourth Annual Conference on Carbon Capture and Sequestration*.

NIELD, D. & BEJAN, A. 1999 *Convection in Porous Media*. Springer.

PARK, J. H., CHUNG, T. J., CHOI, C. K. & KIM, M. C. 2006 The onset of mixed convection in a porous layer heated with constant heat flux. *AIChE J.* **52** (8), 2677–2683.

PEYRET, R. 2002 *Spectral Methods for Incompressible Viscous Flow*. Springer.

PRASAD, A. & SIMMONS, C. T. 2003 Unstable density-driven flow in heterogeneous porous media: A stochastic study of the Elder(1967b) "short heater" problem. *Water Resour. Res.* **39** (1), 1007.

PRUESS, K. 1991 TOUGH2, a general-purpose numerical simulator for multiphase fluid and heat flow. *Report* LBL-29400, Lawrence Berkeley Laboratory.

RIAZ, A., HESSE, M., TCHELEPI, H. A. & ORR JR, F. M. 2006 Onset of convection in a gravitationally unstable diffusive boundary layer in porous media. *J. Fluid Mech.* **548**, 87–111.

ROGERS, F. T. & MORRISON, H. L. 1950 Convection currents in porous media. III: Extended theory of the critical gradient. *J. Appl. Phys.* **21**, 1177.

SCHMID, P. J. 2007 Non-modal stability theory. *Annu. Rev. Fluid Mech.* **39**, 129–162.

SCHMID, P. J. & HENNINGSON, D. S. 2001 *Stability and Transition in Shear Flow*. Springer.

STRAUGHAN, B. 2004 *The Energy Method, Stability and Nonlinear Convection*. Springer.

TAN, C. T. & HOMSY, G. M. 1986 Stability of miscible discplacements in porous media: Rectilinear flow. *Phys. Fluids* **29** (11), 3549.

TREFETHEN, L. N. & EMBREE, M. 2005 *Spectra and Pseudospectra: The Behavior of Nonnormal Matrices and Operators*. Princeton University Press.

XU, X., CHEN, S. & ZHANG, D. 2006 Convective stability analysis of the long-term storage of carbon dioxide in deep saline aquifers. *Adv. Water Resour* **29**, 397–407.

ZYVOLOSKI, G. A., ROBINSON, B. A., WOLFSBERG, A. V., PAWAR, R. J., VISWANATHAN, H., KELKAR, S. & DASH, Z. V. http://fehm.lanl.gov/ Finite element heat and mass transfer code (FEHM). http://fehm.lanl.gov/.